J Physiol Sci (2018) 68:355–367
https://doi.org/10.1007/s12576-017-0538-8

ORIGINAL PAPER

Regulation of the glucose supply from capillary to tissue examined by developing a capillary model

Akitoshi Maeda[1] · Yukiko Himeno[1] · Masayuki Ikebuchi[1] · Akinori Noma[1] · Akira Amano[1]

Received: 28 January 2017 / Accepted: 5 April 2017 / Published online: 17 April 2017

Abstract A new glucose transport model relying upon diffusion and convection across the capillary membrane was developed, and supplemented with tissue space and lymph flow. The rate of glucose utilization (J_{util}) in the tissue space was described as a saturation function of glucose concentration in the interstitial fluid ($C_{glu,isf}$), and was varied by applying a scaling factor f to J_{max}. With $f = 0$, the glucose diffusion ceased within ~20 min. While, with increasing f, the diffusion was accelerated through a decrease in $C_{glu,isf}$, but the convective flux remained close to resting level. When the glucose supplying capacity of the capillary was measured with a criterion of $J_{util}/J_{max} = 0.5$, the capacity increased in proportion to the number of perfused capillaries. A consistent profile of declining $C_{glu,isf}$ along the capillary axis was observed at the criterion of 0.5 irrespective of the capillary number. Increasing blood flow scarcely improved the supplying capacity.

Keywords Mathematical capillary model · Glucose supplying capacity · Diffusion across the capillary membrane · Convective glucose flux · Reflection coefficient

✉ Akinori Noma
noma@sk.ritsumei.ac.jp

[1] Department of Life Sciences, Ritsumeikan University, Shiga, Japan

Introduction

The difference in the glucose concentration between the local arterial and venous blood flow increases with increasing exercise level, indicating that glucose utilization by myocytes is increased [1, 2]. Nevertheless, the microdialysis method did not show an obvious decline in glucose concentration in the interstitial fluid ($C_{glu,isf}$) during physical exercise. Even an increase in $C_{glu,isf}$ above the resting $C_{glu,isf}$ was reported [3]. It has been suggested that this increase in $C_{glu,isf}$ might be attributed to an increase in blood flow during exercise [4]. The increase in $C_{glu,isf}$ was not observed when muscle contraction was evoked by neuromuscular electrical stimulation [3]. Moreover, $C_{glu,isf}$ measured for several hours after an exercise bout was much lower in the exercised leg than in the control rested leg in human experiments [5, 6]. Meanwhile, it is generally believed that glucose transport across the capillary membrane is mostly carried out by diffusion, and the convective transport is small. The driving force for substrate diffusion is the concentration gradient across the membrane. These findings raise the question of how glucose transport across the capillary membrane is increased during muscle exercise. In order to reconcile these experimental findings, quantitative analysis of glucose transport across the capillary membrane is a prerequisite.

Most of the key parameters for both diffusion and convection have been well documented in experimental and theoretical studies [7]. It is now possible to calculate the transcapillary exchange of major substrates based on their permeation coefficients [8] and reflection coefficients [9, 10] across the capillary wall in addition to water permeability [11–13] in combination with Starling's principle. The dependency of lymph flow on tissue volume is also well explained through variation in tissue hydrostatic

pressure [14, 15]. Thus, we await the development of a comprehensive system model composed of capillary, tissue and lymph flow to analyze glucose supply by the capillary. In such models, the interactions, including the positive and negative feedback mechanisms between the solute and the volume exchanges are calculated by solving simultaneous differential equations. However, the number of mathematical models that calculate the substrate exchange across the capillary membrane as well as lymphatic volume transport is still very limited [16–19].

In the present study, we developed a new model composed of capillary, tissue and lymph capillary for skeletal muscle tissue. This model reproduces basic functions of capillary and glucose transport well, via convection as well as diffusion. We have taken an analytical route in solving the question; namely we calculate the glucose flux across a single perfused capillary at varying glucose utilization rates in the tissue (by myocytes). Then, the effects of increasing the number of capillaries or the blood flow are examined to clarify how the glucose supply via the capillaries is adjusted to meet the demand of working muscle. We propose a new criterion to measure the glucose supplying capacity of the capillary as the basis of the muscle work capacity when the number of perfused capillaries or the blood flow is varied. This new capillary model may be applied to various physiological and pathophysiological conditions when studying the balance between glucose demand and supply.

Methods

Model structure

The source code of the model can be downloaded at http://www.eheartsim.com. The present computational model, schematically illustrated in Fig. 1, was developed for a skeletal muscle tissue provided with a continuous type of capillary. Thus, most of the parameters were adopted from experiments in skeletal muscle tissue or organs, such as a hind limb as described below. The capillary space is defined by a single or a few numbers of capillaries. The single capillary unit is 0.6 mm in length and is divided into

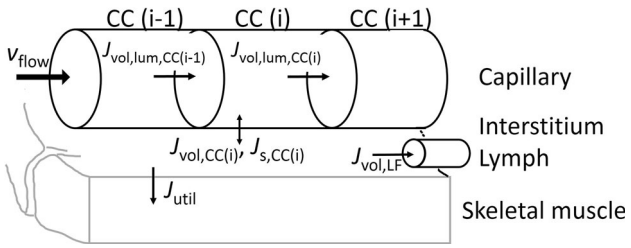

Fig. 1 Model compartments

60 (Nc) compartments along the axis between the arterial and venous ends to calculate the substrate diffusion as well as the convective fluxes with a constant flow rate (v_{flow}) of 1 mm/s [20]. $CC(i)$ is the sequential number of capillary compartments ($i = 1, 2, 3,\ldots 60$). The lymphatic capillary only provides drainage of tissue fluid at a varying flow rate determined as a function of the tissue hydrostatic pressure.

Definitions, dimensions and standard magnitudes of all functional variables are described in Tables 1, 2, 3 and 4.

The model is composed of a single or several capillaries, a lymphatic capillary and an interstitial fluid space (*isf*). Each capillary is divided into 60 compartments (*CC*) along the axis. v_{flow} (mm/ms) is the blood flow velocity. $J_{vol,lum,CC(i)}$ (μl/ms) is the volume flux from $CC(i)$ to $CC(i + 1)$; $J_{vol,lum,CC(i-1)}$ (μl/ms) is the volume flux from $CC(i–1)$ to $CC(i)$; $J_{vol,CC(i)}$ (μl/ms) and $J_{s,CC(i)}$ (plasma protein: g/ms; glucose or NaCl: mmol/ms) are the fluxes of volume and solutes, respectively, across the capillary membrane at the *i*th compartment; and $J_{vol,LF}$ (μl/ms) is the lymphatic drainage of interstitial fluid. J_{util} (mmol/ms) is the glucose utilization flux by hypothetical skeletal myocytes.

The parameters of a single tissue compartment are based on a Krogh cylinder in the skeletal muscle [21, 22], where a cylindrical envelope of muscle tissue was assumed to be supported by the capillary within the Krogh cylinder. The number of perfused capillaries can vary, depending on the metabolic condition of the tissue or the influence of systemic regulation. The *isf* was assumed to be 13% of the Krogh cylinder and the rest was assumed to be occupied by the capillary and surrounding parenchymal cells.

The saturation kinetics of glucose utilization as determined by the rate limiting glucose uptake into skeletal myocytes

Holloszy and Narahara [23] showed that the uptake of sugar into stimulated muscle exhibits a saturation type of kinetics, and the increase in permeability is related more to a change in maximum rate of uptake (V_{max}) than in the half-saturation concentration ($K_{0.5}$). This glucose transport across the cell membrane is a major rate-limiting step in glucose utilization in skeletal muscle cells [24]. Although a shift of the rate-limiting step from membrane transport toward phosphorylation of glucose was observed in insulin-stimulated red muscle, Furler et al. [25] concluded that the membrane transport step dominates muscle glucose utilization. Supporting this view, Ziel et al. [26] found that intracellular free glucose does not accumulate in skeletal muscle.

Skeletal muscle membrane glucose transport is due to facilitated diffusion via GLUT4, which is increased in number on the surface cell membrane under the influence of insulin-mediated signal transduction [27], or by some

Table 1 Definition of variables

Symbols	Definitions	Units
C	Substrate concentration	mmol/l
f	Scaling factor of the maximum rate of consumption	–
I_s	Index of saturation	–
Q	Quantity of substrate movement	mmol
P	Hydrostatic pressure	mmHg
P_e	Effective pressure	mmHg
π	Osmotic pressure	mmHg
J	Flux	µl/ms, g/ms or mmol/ms
v	Velocity	mm/ms or mmol/ms

Table 2 Subscripts

Symbols	Definitions
s	Substrate (plasma protein, glucose, NaCl)
pp	Plasma protein
glu	Glucose
NaCl	NaCl
LF	Lymph flow
Vol	Volume
CC(i)	ith capillary compartment (i = 1, 2, 3,…60)
isf	Interstitial fluid space
pl	Plasma
a	Arterial end of capillary
v	Venous end of capillary
lum	Luminal side of capillary
conv	Convection
diff	Diffusion
filt	Filtration
reab	Reabsorption
r	Reference
max	Maximum
util	Utilization

intrinsic cellular mechanisms [28, 29]. Moreover, under the regulation of the central nervous system, skeletal muscle activity is increased by increasing the number of active fraction of motor units. Based on these findings, we calculated the rate of glucose utilization (J_{util}) in the model tissue space using a saturation function [Eq. (1)] [23, 24]. Here, the glucose 'utilization' includes two steps: transmembrane transport and intracellular metabolism.

$$J_{util} = \frac{J_{max}}{1 + \frac{K_{0.5}}{C_{glu,isf}}}. \quad (1)$$

Here, J_{max} represents the maximum glucose uptake, which is given by the product of total number of transporters (GLUT4) times the turnover rate of the carrier. The total number of transporters is proportional to both the density of GLUT4 on the myocytes and the number of active motor units. Thus, in the presented simulation model, J_{max} is increased when the muscle is activated. We tentatively used a value of $K_{0.5}$ (=3.5 mM) of GLUT4 [30]. To represent changes in J_{util} in the tissue space, J_{max} in Eq. (1) was given by a product of reference J_{max} ($J_{max,r}$) and a scaling factor (f). We obtained $J_{max,r}$ at rest ($J_{max,r} = 7.75 \times 10^{-16}$ mmol/ms) using values of $C_{isf,r}$ (4.7 mM) and $J_{util,r}$ (1.4×10^{-3} mmol glucose/min/100 g tissue) measured in the resting muscle [22].

$$J_{util} = \frac{f \cdot J_{max,r}}{1 + \frac{K_{0.5}}{C_{glu,isf}}}. \quad (2)$$

Then, an index of saturation (I_s) was determined by Eq. (3) at each f. $J_{max,r}$.

$$I_s = \frac{J_{util}}{f \cdot J_{max,r}} = \frac{1}{1 + \frac{K_{0.5}}{C_{glu,isf}}}. \quad (3)$$

To measure the glucose supplying capacity of the capillary as the basis of the work capacity of skeletal muscle, we apply a new criterion level 0.5 to I_s and determine the magnitude of the scaling factor f ($f_{0.5}$), which gives $I_s = 0.5$ at a given number of capillaries or a blood flow. It will be shown in the Results Section that the glucose supplying capacity, represented by $f_{0.5}$ increases when the number of perfused capillaries is increased.

Hydrostatic pressure of capillary and tissue

The hydrostatic pressure $P_{CC(i)}$ in a $CC(i)$ was defined as a linear function of the axial number i in Eq. (4). A standard arterial pressure (P_a) of 25 mmHg and a venous P_v of 15 mmHg were assumed.

$$P_{CC(i)} = P_a + (P_v - P_a) \cdot \frac{i}{N_c} \quad (4)$$

Table 3 Parameters of the model

Symbols	Definitions	Values	Units
a	Degree of dissociation	NaCl: 1.87, Glucose: =1	–
A_{CC}	Area of cross section of capillary	5.027×10^{-5}	mm^2
A_s	Surface area of a capillary compartment	2.513×10^{-4}	mm^2
D_s	Diffusion coefficient of substrates	D_{pp}: 1.40×10^{-4}, D_{glu}: 1.54×10^{-7}, D_{NaCl}: 2.47×10^{-7} (9)	mm^2/ms
$K_{0.5}$	Half saturating glucose concentration	3.5 (30)	mmol/l
I_{CC}	Length of a capillary compartment	0.01	mm
L_P	Hydraulic conductivity of capillary membrane	1.54×10^{-9} (34)	mm/ms mmHg
N_c	Number of capillary compartments	60	–
p_s	Substrate permeability coefficient	p_{pp}: 4.73×10^{-13}, p_{glu}: 1.0×10^{-10}, p_{NaCl}: 3.60×10^{-10} (8)	mm/ms
E	Gas constant	62.4×10^{-3}	mmHg l/K/mmol
T	Absolute temperature	310	K
σ_s	Reflection coefficient for substrate	σ_{pp}: 0.973, σ_{glu}: 0.066, σ_{NaCl}: 0.054 (9)	–
η	Viscosity of the serum	0.004	N ms/mm^2

Numbers in parenthesis indicate references

Table 4 Initial values

Symbols	Definitions	Values	Units
$C_{pp,CC(i)}$	Concentration of plasma protein in capillary	75.9	g/l
$C_{s,CC(i)}$	Concentration of substrates in capillary	C_{glu}: 5 C_{NaCl}: 150	mmol/l
$C_{pp,isf}$	Concentration of plasma protein in interstitial fluid	17.6	g/l
$C_{s,isf}$	Concentration of substrates in interstitial fluid	C_{glu}: 4.71 C_{NaCl}:149	mmol/l
K_B	Boltzmann constant	1.38×10^{-23}	J/K
P_a	Blood pressure at arterial end	25	mmHg
P_v	Blood pressure at venous end	15	mmHg
P_{isf}	Hydrostatic pressure in interstitial space	−1.08	mmHg
v_{flow}	Velocity of plasma flow	1	mm/s
$V_{CC(i)}$	Volume of *i*th capillary segment	5.03×10^{-7}	µl
V^0_{isf}	Original volume of interstitial space	3.18×10^{-4}	µl
V_{isf}	Volume of interstitial space at control	3.68×10^{-4}	µl
J_{max}	Standard rate of glucose consumption	7.75×10^{-16}	mmol/ms
$\pi_{s,CC}$	Colloid osmotic pressure of capillary	See text	mmHg
$\pi_{s,isf}$	Osmotic pressure of interstitial space	See text	mmHg

The interstitial hydrostatic pressure P_{isf} is subatmospheric in most tissues [31]. The interstitial volume-pressure relation (compliance curve) was represented by a sigmoidal function of V_{isf}/V^0_{isf}, where V^0_{isf} is a reference volume of *isf*. The parameters were determined by fitting an equation [Eq. (5)], which includes an exponential and a linear terms, to the experimental data obtained in canine hind limbs [32], shown in Fig. 2a.

$$P_{isf} = -e^{-(rVisf-1.07)/0.0953} + (1.4 \cdot rV_{isf} - 2.38), \quad rV_{isf} = \frac{V_{isf}}{V^0_{isf}}. \tag{5}$$

The magnitude of V^0_{isf} was determined as 13% of a Krogh muscle cylinder of dimensions 0.6 mm in length and 0.036 mm in radius [21].

Lymph flow

The tissue hyrostatic pressure given by Eq. (5) is the major factor in driving lymphatic drainage of *isf*, $J_{vol,LF}$ (l/ms). The dependency of $J_{vol,LF}$ on the P_{isf} obtained in the hind limb preparation [14] is cited in Fig. 2b, and was fitted with the empirical Eq. (6)

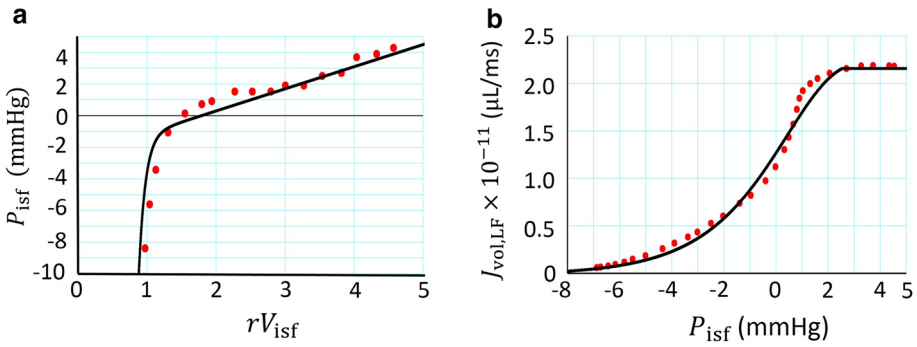

Fig. 2 Model fitting of the experimental volume-pressure relation (**a**) [32], and the pressure-lymph flow relationships (**b**) [14]. *Dots* are experimental measurements in the hindlimb preparation, and the *continuous curve* is the theoretical relationship of Eq. (5) and Eq. (6)

$$J_{\mathrm{vol,LF}} = \frac{9 \times 10^{-11}}{e^{\frac{P_{\mathrm{isf}}+6.08}{-2.16}} + e^{\frac{P_{\mathrm{isf}}-18.9}{4.5}}}. \tag{6}$$

Colloid and crystalloid osmotic pressures

The colloid osmotic pressure π_{pp} (mmHg) is a function of plasma protein (pp) concentration C_{pp} (g/l) as exemplified in an experimental finding [33], and was determined by fitting an empirical Eq. (7). Equation (7) was applied to both the plasma and tissue compartments.

$$\pi_{\mathrm{pp}} = 0.21 \cdot C_{\mathrm{pp}} + 0.0016 \cdot C_{\mathrm{pp}}^2. \tag{7}$$

The crystalloid osmotic pressure π_{s} caused by a substrate s (glucose or NaCl) was determined by van 't Hoff's law [Eq. (8)], where R is the gas constant, T is the absolute temperature, C is concentration, and α is the degree of dissociation. The values of α are 1.0 and 1.87 for glucose and NaCl, respectively [9].

$$\pi_{\mathrm{s}} = R \cdot T \cdot C_{\mathrm{s}} \cdot \alpha\, s;\ \{\mathrm{NaCl,\ glucose}\}. \tag{8}$$

Fluid volume and solute fluxes between successive capillary compartments

The volume flux $J_{\mathrm{vol,lum,CC}(i)}$ between the (i–1)th and the ith compartments is described using Eq. (9).

$$J_{\mathrm{vol,lum,CC}(i)} = V_{\mathrm{CC}(i-1)} \cdot \frac{v_{\mathrm{flow}}}{l_{\mathrm{cc}}}, \tag{9}$$

where $V_{\mathrm{CC}(i-1)}$ is the volume of capillary $(i–1)th$ compartment, l_{cc} is the length of a capillary compartment and v_{flow} is velocity of blood flow. The substrate flux across the boundary between two successive capillary compartments $J_{\mathrm{s,lum,CC}(i)}$ (i–1) and i was calculated as a sum of diffusion and convection terms in Eq. (10).

$$J_{s,\mathrm{lum,CC}(i)} = D_s \cdot A_{cc} \cdot \left\{C_{s,\mathrm{CC}(i-1)} - C_{s,\mathrm{CC}(i)}\right\} + J_{\mathrm{vol,lum,CC}(i-1)} \cdot C_{s,\mathrm{CC}(i-1)} \tag{10}$$

s; {pp, glucose, NaCl}.

We corrected diffusion coefficient D (mm^2/ms) for T (K), and viscosity (η) of the serum (=0.004 N ms/mm^2) using the Stoke–Einstein relation [Eq. (11)].

$$D = \frac{K_b \cdot T}{6\pi\eta\gamma}, \tag{11}$$

where K_b is the Boltzmann constant (=1.38 × 10^{-23} J/K), π is the circular constant (=3.14) and γ (mm) is the Stokes–Einstein radius of the molecule [9]. For γ, we referred to Rippe and Haraldsson [9]. Thus, D_{alb}: 1.40 × 10^{-4}, D_{glu}: 1.54 × 10^{-7}, and D_{NaCl}: 2.47 × 10^{-7} were obtained. These values are nearly comparable or slightly smaller than those used by Kellen et al. [17], which were D_{alb}: 1.53 × 10^{-4}, D_{sucrose}: 7.0 × 10^{-7}, D_{NaCl}: 2.0 × 10^{-6}. On the other hand, the parameters in Kellen et al. [17] are rather similar to the diffusion coefficient in water.

Fluid volume and solute fluxes across the capillary membrane

The volume flux across the capillary membrane $J_{\mathrm{vol,CC}(i)}$ for a single capillary compartment was calculated by the Starling principle extended for crystalloid osmotic pressures [Eq. (12)]. Note that the third factor gives the effective filtration pressure P_{e} defined in Starling's principle.

$$J_{\mathrm{vol,CC}(i)} = L_p \cdot A_s \cdot \left[\left\{P_{\mathrm{CC}(i)} - P_{\mathrm{isf}}\right\} - \sum_s \left\{\sigma_{\mathrm{s}}\left(\pi_{\mathrm{s,CC}(i)} - \pi_{\mathrm{s,isf}}\right)\right\}\right], \tag{12}$$

where L_p is the hydraulic conductivity of the capillary membrane, A_{s} is the capillary surface area, and $P_{\mathrm{CC}(i)}$ and P_{isf} are the hydrostatic pressures in the capillary compartment $CC(i)$ and interstitial space, respectively. The reflection coefficient for a solute s is σ_{s} ($\sigma_{\mathrm{pp}} = 0.973$, $\sigma_{\mathrm{glu}} = 0.066$, $\sigma_{\mathrm{NaCl}} = 0.054$) [9], and $\pi_{\mathrm{s,CC}(i)}$ and $\pi_{\mathrm{s,isf}}$ are osmotic pressures in $CC(i)$ and interstitial space, respectively.

We determined the water permeability (L_p) of the capillary membrane from the experimental data described in 'Textbook of Medical Physiology' [34], in which Guyton wrote that '13 mmHg filtration pressure causes, on average, about 1/200 of the plasma in the flowing blood to filter out of the arterial ends of the capillaries into the interstitial spaces each time the blood passes through the capillaries'. Assuming an arterial end of 0.3 mm in length, blood passing through the arterial end within 300 ms, and a hematocrit of 0.4, a L_p of 1.54×10^{-9} (mm/ms/mmHg) is obtained. In the frog mesentery, values for L_p of 1.36×10^{-8} [11] and 4.06×10^{-9} [35] were reported. In the human forearm, a L_p of 1.66×10^{-10} [36], and in rat skeletal muscle a L_p of 9.97×10^{-10} [37], and 3.32×10^{-10} [13] have been reported. Thus, the magnitude of L_p in the present model is within the range of variation.

The solute flux $J_{s,CC(i)}$ (g/ms or mmol/ms) across a capillary membrane of a compartment $CC(i)$ was determined as a sum of diffusion $J_{s,diff,CC(i)}$ and convection $J_{s,conv,CC(i)}$ [38]:

$$\begin{aligned} J_{s,CC(t)} &= J_{s,diff,CC(i)} + J_{s,conv,CC(t)} \\ &= p_s \cdot A_s \cdot (C_{s,CC(i)} - C_{s,isf}) + J_{vol,CC(i)} \cdot C_{s,x} \cdot (1 \\ &\quad - \sigma_s)\, x \\ &: \{CC(i), isf\}, \end{aligned} \tag{13}$$

where A_s is the surface area for diffusion, and $C_{s,CC(i)}$ or $C_{s,isf}$ is concentration of substrate s in the volume flux $J_{vol,CC(i)}$ across the capillary wall.

For the permeability p_s (mm/ms) across the capillary membrane, we referred to Renkin [8] and Levick [22], and defined a p_{pp} of 4.73×10^{-13}, p_{glu} of 1.0×10^{-10}, and p_{NaCl} of 3.60×10^{-10}. These values are similar to those used in the Kellen model; p_{alb}: 4.3×10^{-12}, $p_{sucrose}$: 2.6×10^{-10}, p_{NaCl}: 8.1×10^{-10}.

Ordinary differential equations to determine rate of volume and concentration changes

Changes in the interstitial and capillary volumes and the quantity of substrate (Q) were calculated by the numerical time integration of the transcapillary exchange of fluid (dV/dt) and solute (dQ_s/dt) using the Euler method.

$$\frac{dV_{CC(i)}}{dt} = J_{vol,lum,CC(i-1)} - J_{vol,lum,CC(i)} - J_{vol,CC(i)} \tag{14}$$

$$\frac{dV_{isf}}{dt} = \sum_{i=1}^{Nc} \{J_{vol,CC(i)}\} - J_{vol,LF} \tag{15}$$

$$\frac{dQ_{s,CC(i)}}{dt} = J_{s,lum,CC(i-1)} - J_{s,lum,CC(i)} - J_{s,CC(i)} \quad s; \{pp, NaCl, glucose\} \tag{16}$$

$$\frac{dQ_{s,isf}}{dt} = \sum_{i=1}^{Nc} \{J_{s,CC(i)}\} - J_{vol,LF} \cdot C_{s,isf} \quad s; \{pp, NaCl\} \tag{17}$$

$$\frac{dQ_{glu,isf}}{dt} = \sum_{i=1}^{Nc} \{J_{glu,CC(i)}\} - J_{vol,LF} \cdot C_{glu,isf} - J_{util}. \tag{18}$$

Results

Glucose supply to *isf* space via convection and diffusion

It has been suggested that the glucose supply to the skeletal myocytes is largely carried out by diffusion [22, 39]. Our new capillary model examines the amplitude of glucose diffusion flux ($J_{glu,diff} = \sum J_{glu,diff,CC(i)}$) and the convective flux ($J_{glu,conv} = \sum J_{glu,conv,CC(i)}, J_{glu,filt} = \sum J_{glu,filt,CC(i)}, J_{glu,reab} = \sum J_{glu,reab,CC(i)}$) across the capillary membrane as shown in Fig. 3. The four factors of Starling's principle are demonstrated in Fig. 3a against sequential capillary compartment number at the resting level of glucose utilization in the tissue space. $\pi_{pp,CC(i)}$ (blue) is quite uniform in all segments of the capillary because of the large reflection coefficient for pp. In Fig. 3b, $J_{vol,CC(32)}$ was µl/ms and the net volume flux J_{vol} was slightly positive (not shown), and was balanced by the negative lymph flow (black line in Fig. 3b).

Figure 3c1 shows the convective glucose flux $J_{glu,conv,CC(i)}$ by filtration (red), and absorption (blue) in each compartment of the capillary for comparison with the diffusion flux $J_{glu,diff,CC(i)}$ (black line), which is virtually uniform for all capillary components. The $J_{glu,conv,CC(i)}$ is quite proportional to the fluid flux $J_{vol,CC(i)}$ (Fig. 3b, c1), since the difference in C_{glu} is relatively small between capillary and tissue. In this respect, the profile of $J_{glu,conv,CC(i)}$ (Fig. 3c1) is similar to $J_{NaCl,conv,CC(i)}$ (Fig. 3c3), but in strong contrast to $J_{pp,conv,CC(i)}$, showing a marked asymmetry between filtration and reabsorption, because of the large difference between $C_{pp,CC(i)}$ and $C_{pp,isf}$ (Fig. 3c2).

The capillary factors $\pi_{pp,CC(i)}$ and $P_{cc(i)}$ remain virtually constant during various simulation conditions in the present study. On the other hand, the tissue parameters π_{isf} and P_{isf} change in a dynamic manner, and are mainly responsible for adjusting the convective glucose flux in response to various experimental conditions.

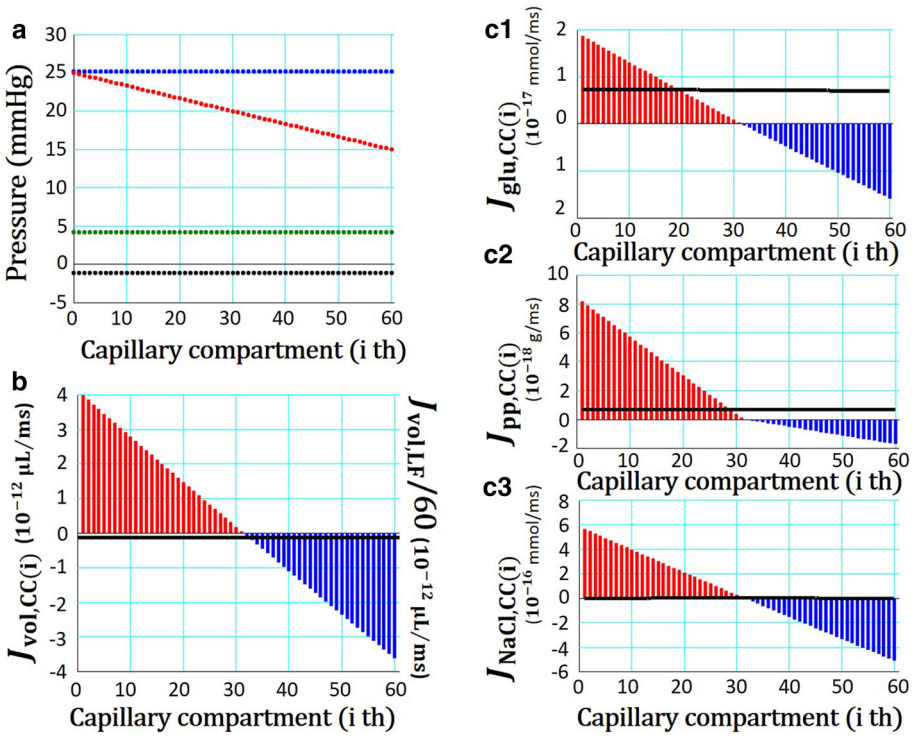

Fig. 3 Main factors involved in the glucose flux under the control (resting) condition. **a** Capillary colloid osmotic pressure $\pi_{pp,CC(i)}$ (*blue*), capillary hydrostatic pressure $P_{CC(i)}$ (*red*), tissue colloid osmotic pressure $\pi_{pp,isf}$ (*green*), and tissue hydrostatic pressure P_{isf} (*black*). **b** The volume flux across the capillary membrane: the filtration $J_{vol,filt,CC(i)}$ (*red*) and reabsorption $J_{vol,reab,CC(i)}$ (*blue*). The lymphatic drainage of interstitial fluid $J_{vol,LF}$ is indicated by a *black line,* all in a dimension of 10^{-12} µl/ms. **c1**, **c2**, **c3** The solute convective flux $J_{s,conv,CC(i)}$ by filtration (*red*) and reabsorption $J_{s,conv,CC(i)}$ (*blue*). **c1** Glucose flux (10^{-17} mmol/ms), **c2** plasma protein flux (10^{-18} g/ms), and **c3** NaCl flux (10^{-16} mmol/ms). The diffusion fluxes $J_{s,diff,CC(i)}$ are indicated by a *black line* in each graph

Balance between diffusional glucose supply and cellular glucose utilization during exercise

If glucose utilization (J_{util}) by the tissue was nullified, the glucose gradient across the capillary membrane dissipated, and $J_{glu,diff}$ totally disappeared within ~20 min, indicating that glucose diffusion was indirectly driven by J_{util} (Fig. 4a). On the other hand, an increase in tissue J_{util} during exercise greatly increased $J_{glu,diff}$. In Fig. 4b, J_{util} was increased by augmenting J_{max} by 20-fold [i.e., changing f to 20 from 1 in Eq. (2)] at 50 min. This intervention caused an immediate rise of J_{util} (blue curve in Fig. 4b1) close to the target J_{util} level (black line), which was determined by f (=20) and the initial $C_{glu,isf}$ (=4.7 mM) (Eq. 2). Then, J_{util} started to decrease to a new steady level (57% of the initial level) by the decrease in $C_{glu,isf}$ to less than 2 mM as indicated in Fig. 4b2 (black curve). This decrease in $C_{glu,isf}$ largely magnified $J_{glu,diff}$ until the net glucose flux across the capillary membrane, subtracted by the glucose removal via lymph flow (red curve in Fig. 4b1) matched the augmented J_{util} (blue curve) well at around 50 mmol/ms ~15 min after switching f to 20.

When $f.J_{max}$ was returned to the control level by switching f to 1 from 20 at 150 min, a reverse sequence of events occurred to recover the control levels of each variable within 15 min.

The decrease in $C_{glu,isf}$ during the period of accelerated J_{util} largely lowered π_{isf} and decreased V_{isf}, as shown in Fig. 4b3, and thereby $C_{pp,isf}$ was secondarily increased as shown by the red trace in Fig. 4b2. On the other hand, the $C_{NaCl,isf}$ remained at the control level (blue trace in Fig. 4b2), because of its high conductivity across the capillary membrane. The slow process of re-equilibration of pp, however, caused a drift of $C_{pp,isf}$ and caused delayed recovery of the V_{isf} as shown in Fig. 4b3. These changes in the tissue parameters were completely reversible.

The magnitude of $J_{glu,diff}$ (red curve) is compared with $J_{glu,conv}$ (filtration, yellow and absorption purple) in more detail in Fig. 4b1. During the control, the magnitude of glucose supply to *isf* due to filtration $J_{glu,filt}$ was nearly comparable (~70%) to $J_{glu,diff}$. This magnitude of $J_{glu,filt}$ remained almost unchanged during the high J_{util} period because the fluid flux was not significantly modulated by the increase in J_{util}. On the other hand, $J_{glu,reab}$ (purple) was decreased by the depletion of $C_{glu,isf}$, thereby the net convective flux of glucose was increased during exercise, although the magnitude was much smaller than the

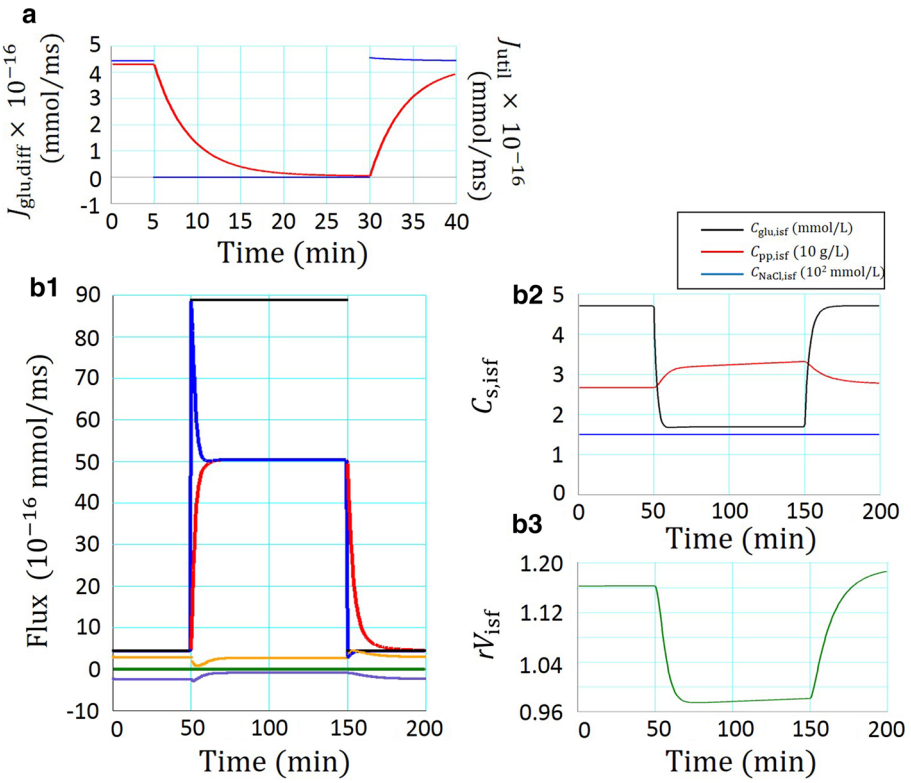

Fig. 4 Time course of the glucose transport response evoked by varying the metabolic activity (**a** $f = 0$, **b** $f = 20$) in the tissue space. **a** Cessation of glucose diffusion ($J_{glu,diff}$) after nullifying J_{util} through equilibration of glucose concentration between capillary and *isf*. The glucose utilization J_{util} (*blue*) and the net glucose transport $J_{glu,\ diff}$ (red) are shown. **b1** Glucose flux J_{glu} across the capillary membrane given in 10^{-16} mmol/ms. The target J_{util} determined by f (=20) and the initial $C_{glu,isf}$ (=4.7 mM) (Eq. 2) (*black*), the evolution of J_{util} (*blue*), the net glucose transport $J_{glu,diff}$ (*red*), glucose filtration transport $J_{glu,filt}$ (*yellow*), glucose reabsorption transport $J_{glu,\ reab}$ (*purple*), and lymphatic glucose drainage of interstitial fluid $J_{glu,\ LF}$ (*green*) are shown. **b2** Interstitial concentration of $C_{glu,isf}$ (mmol/l, *black*), $C_{pp,isf}$ (10 g/l, *red*) and $C_{NaCl,isf}$ (10^2 mmol/l, *blue*). **b3** Relative tissue volume ($rV_{isf,}$ *green*). On returning to the control condition, rV_{isf} showed a rebound because of an accumulation of *pp* during the test period of $f = 20$

diffusional flux. It is concluded that the increase in J_{util} during heavy exercise is largely compensated for by $J_{glu,diff}$.

Adjustments of glucose supply by increasing the number of capillaries and velocity of blood flow

The increase in J_{util} in response to heavy exercise as demonstrated in Fig. 4b was examined over a wide range of f (Fig. 5). Within a range of approximately $0 \sim 5$ times f, it seems that J_{util} increased in proportion to f. However, the relationship is evidently a saturating function; the ratio $J_{util}/(f \cdot J_{max,r})$ gradually decreased with increasing f (red curve in Fig. 5). This finding might suggest that the glucose supply to the skeletal muscle by capillary becomes deficient and the work capacity is decreased, when the exercise level is raised. Under the condition in situ this shortage of glucose supply is compensated for by the autonomous increase in the number of perfused capillaries. This situation was simulated by increasing the number of capillaries for the model tissue compartment. As shown in

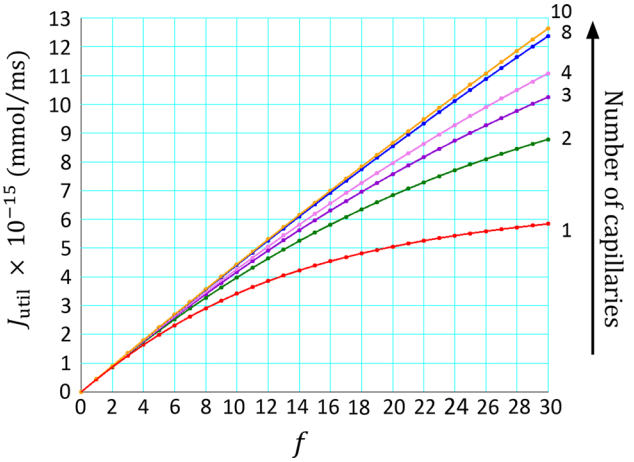

Fig. 5 The relation between J_{util} and the scaling factor f of $J_{max.r}$ at different numbers of capillaries indicated at the *right side*

Fig. 5, the J_{util} was much increased with increasing number of capillaries, with an obvious trend of saturation in the effect.

An alternative way of increasing the glucose supply might be applied by accelerating the velocity of the blood flow through the capillary. This possibility was examined as shown in Fig. 6. Surprisingly, however, effects of increasing the flow rate were very limited. On the other hand, if the flow rate was decreased to 0.1 mm/s, $C_{glu,CC(i)}$ gradually declined with increasing compartment number by ~0.14 mM at the venous end. A marked decay in the $C_{glu,CC(i)}$ profile was obtained when the flow rate was further decreased to 0.01 to simulate profound ischemia [40]. The decrease in the $C_{glu,CC(i)}$ profile was largely compensated for by increasing the number of capillaries threefold (Fig. 6c).

The capacity of capillaries for supplying glucose measured by applying a criterion of 0.5 to the saturation index I_s

Using the criterion of $I_s = 0.5$, the glucose supplying capacity was measured from the magnitude of $f_{0.5}$ at a given number of capillaries. Figure 7a shows the relationship between I_s on the abscissa and $C_{glu,isf}$ on the ordinate. The five relationships between the scaling factor f (on the abscissa) and the steady-state $C_{glu,isf}$ (on the ordinate) were determined at different numbers of capillaries as indicated with different colors. Thus, $f_{0.5}$ is indicated by the arrowheads drawn from each intersection of the horizontal line of $I_s = 0.5$ with individual curves of $C_{glu,isf}$. It is evident that the $f_{0.5}$ increased with increasing number of perfused capillaries. Namely, the magnitude of $f_{0.5}$ was increased to 5.96, 11.9 and 17.8 with the number of capillaries = 1, 2 and 3, respectively (Fig. 7b), indicating that the $f_{0.5}$ increases in proportion to the number of capillaries within a single tissue space. That is, the glucose supplying capacity of the capillaries was magnified in proportion to the capillary number. This proportional increase in the glucose supplying capacity was obtained when the criterion level of I_s was varied within a range of 0.3 ~ 0.57. Most probably, the work capacity of muscle might be simultaneously augmented in proportion to the capillary number.

It is also evident that the steady-state level of $C_{glu,isf}$ was raised with increasing number of capillaries. This finding is consistent with the measurements of $C_{glu,isf}$, which increased with increasing workload of the muscle [3], provided that the number of perfused capillaries was increased by the local as well as systemic regulations. It should be noted that glucose diffusion across the capillary membrane is still well driven by the difference between $C_{glu,CC(i)}$ and $C_{glu,isf}$ in Fig. 7b.

The I_s (Fig. 7a) or f (Fig. 7b) were plotted on each abscissa against the common ordinate of $C_{glu,isf.}$. Different colors in Fig. 7b indicate the different number of capillaries assumed within the tissue space, as indicated on the right side of the figure. In Fig. 7b, the $C_{glu,isf}$ at $f = 0$ is equal to the $C_{glu,CC(i)}$.

When the blood flow was increased to 0.01, 0.1, 1 and 4 (mm/s) in the single capillary, the capacity of supplying glucose ($f_{0.5}$), was increased to 1.22, 4.72, 5.96 and 6.03, respectively (data not shown). Obviously, the glucose supplying capacity was saturated at $v_{flow} > 1$ mm/s.

The findings described so far indicate that the $C_{glu,CC(i)}$ profile reflects the glucose supplying capacity of the capillary well. This notion was further tested by plotting the $C_{glu,CC(i)}$ profile along the axis of the capillary obtained using the criterion of $I_s = 0.5$ with various numbers of perfused capillaries. As shown in Fig. 8, the $C_{glu,CC(i)}$ profiles at $I_s = 0.5$ were superposable at one (black points), two (red) and three (green) capillaries. Thus, the value of $f_{0.5}$ defines a unique set of $C_{glu,CC(i)}$ and $C_{glu,isf}$. These

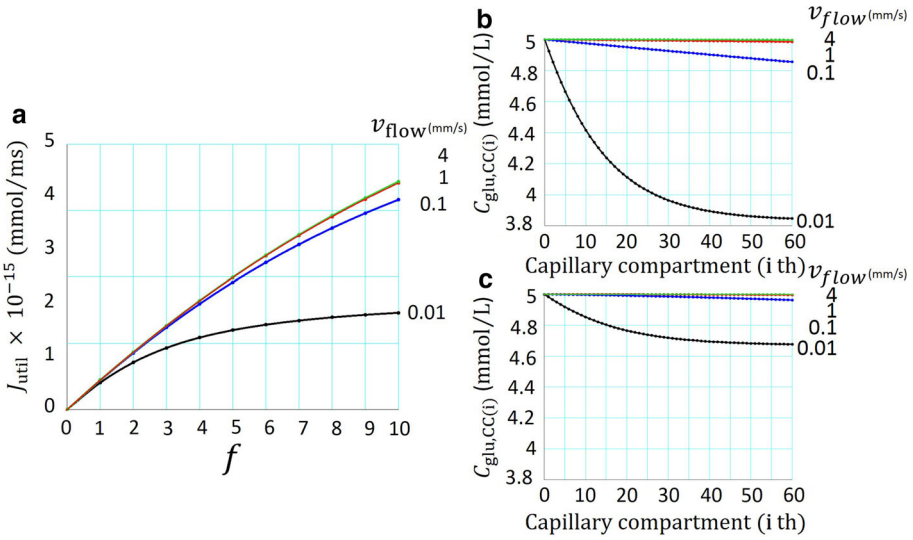

Fig. 6 The J_{util}-f relations (**a**) and the profiles of $C_{glu,CC(i)}$ along the capillary axis when the numbers of capillaries were one (**b**) and three (**c**), respectively. **a** v_{flow} was varied by fourfold (*green*), onefold (control, *red*), 0.1-fold (*blue*) and 0.01-fold (*black*). The J_{util}-f relations were nearly superimposed. **b** Profiles of $C_{glu,CC(i)}$ along the capillary axis when the capillary number was one. **c** The same profiles of $C_{glu,CC(i)}$ obtained when the capillary number was three

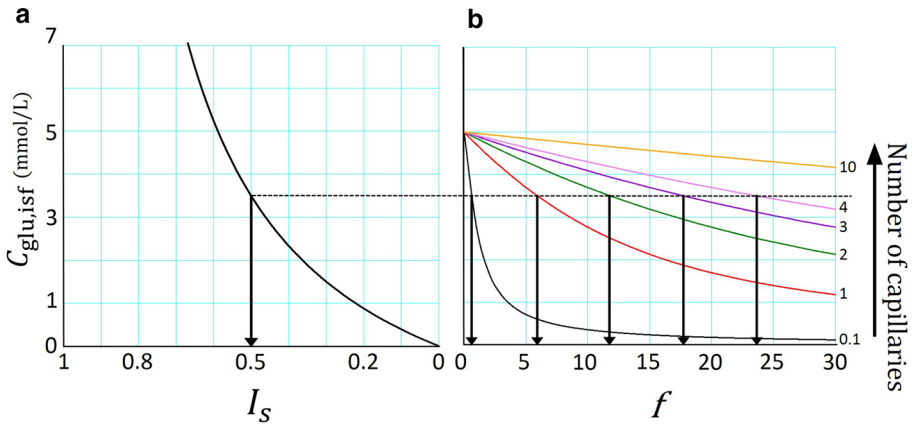

Fig. 7 The steady-state relationship between the I_s (**a**) and f (**b**) as revealed by the *horizontal line* drawn at the criterion level $I_s = 0.5$

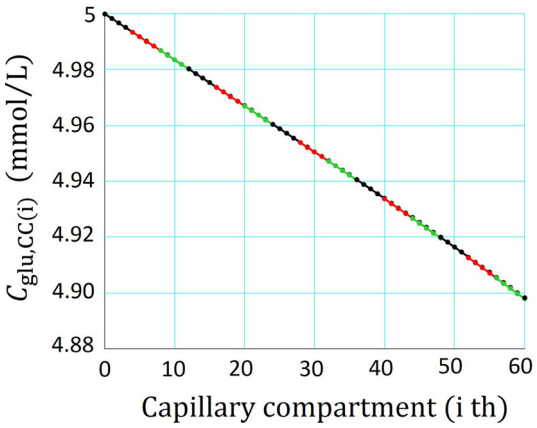

Fig. 8 The profile of $C_{glu,CC(i)}$ along the capillary axis at $I_s = 0.5$. The values of f were 8.74 at one (*black*), 17.5 at two (*red*) and 26.2 at three capillaries (*green*). For better visibility, the three curves, nearly identical, were plotted in an alternating way with different colors

results prove the relevance of using the criterion of $f_{0.5}$ in evaluating the capillary capability to provide glucose. It should be noted that the overlap of the $C_{glu,CC(i)}$ profiles only occurs when the diffusion flux dominates over the convective glucose flux, since the convective flux is almost independent from $C_{glu,isf}$.

Discussion

Relevance of the presented capillary model

The histological composition of the model was determined according to a Krogh cylinder in skeletal muscle. The biophysical parameters, such as the reflection coefficients, the colloid, as well as the crystal osmotic pressures, the diffusion conductivity of various substrates and conductivity of water across the capillary membrane are all based on experimental data obtained in skeletal muscle tissue or organs, as described in the Method. The magnitude of the lymph flow as a function of the tissue hydrostatic pressure has also been well measured in the canine hind limb [32]. The presented model based on those experimental measurements simulated the supply of glucose to the skeletal muscle well at varying levels of muscle activities scaled by f. The present model study confirmed that the glucose supply to tissue cells largely depends on glucose diffusion across the endothelial wall. When the glucose supplying capacity of the capillary is measured with the criterion $f_{0.5}$ defined by the saturation kinetics, the capacity was increased in proportion to the number of perfused capillaries; in other words, in proportion to the glucose diffusion area of the capillary. This simulation model substantiated by the criterion of $f_{0.5}$ might be relevant to evaluation of the capillary capacity for supplying glucose in the intact tissues or most probably to evaluate the increase in the work capacity of the muscle, induced by increasing the number of perfused capillaries.

The convection flux of glucose across the capillary wall

The evaluation of the convection flux of glucose in the present study should be thoroughly discussed in respect to the water flux, which was calculated by the classic Starling principle. It has been suggested that the fluid balance is not directly determined by the plasma protein concentration in the interstitial fluid, but that the concentration just below the filtration structure (underneath space), glycocalyx sheet, should be used in calculating the fluid balance [41–43]. The detailed quantitative studies strongly suggested that the concentration of protein in a local space just beneath the glycocalyx sheet should be lower than that in the bulk interstitial space by about 30% [44]. This is because ultrafiltrate through the glycocalyx toward the tissue side inhibits the back diffusion of protein molecule from the bulk tissue space to the underneath space. This effect should be dependent on the flow rate of filtrate through the narrow gap (~4 nm, [44]) of tight junctional

strand, where the flow rate is much accelerated. They measured the effective oncotic pressure across rat mesenteric microvessels with and without albumin in the interstitial fluid. They found the effective oncotic pressure was near 70% of the luminal oncotic pressure when the albumin concentrations were equal across the endothelial wall. Thus, the ratio of $J_{glu,conv}$ and $J_{glu,diff}$ might be only marginally modified, but the major role of diffusional flux in supplying glucose at enhanced tissue activity remains as estimated in the present study.

At the venous end of the capillary, reabsorption of fluid might also be modified if pp is accumulated in the underneath space by the flow directed from the bulk to the underneath space [45]. At present, however, quantification of this effect is beyond the scope of the present study.

Involvement of the gel structure in the tissue colloid pressure

One of the major comprehensive microcirculation models was published by Kellen et al. [16, 17] for the cardiac muscle. Most of the model parameters are similar to the presented model, except those parameters which are specific for the cardiac tissue; such as the hydraulic pressure of the tissue. In the cardiac muscle there is a huge gradient of hydraulic pressure in the tissue between the epicardial and endocardial sides. In the endocardial muscle layer, the tissue hydrostatic pressure is similar to the pressure in the ventricular cavity during systole, and this effect of systolic pressure is minimal on the epicardial side of the muscle tissue.

The colloid osmotic pressure in the interstitial fluid is much higher ($\sim$25 mmHg) in the Kellen model than in our skeletal muscle model. This high colloid osmotic pressure in the Kellen model was attributed to the matrix protein. However, this colloid osmotic pressure is largely different to the detailed analysis based on the glycocalyx theory described above, or the hypothesis of Guyton [31]. Note that the fluid balance across the glycocalyx layer was determined only by assuming the freely diffusive protein in the underneath space bordered by the tight junction strand underneath the glycocalyx. The involvement of the matrix proteins, such as proteoglycan was not considered in this space. Guyton assumed a 2 mmHg oncotic pressure at most, when the gel is included in a bag made by a filtration membrane, where the glycosaminoglycan is not freely diffusive, but is restrained by the cross-linkage within the gel structure. However, it is unlikely that the gel structure extends to the glycocalyx membrane through the gap of the tight junction strand. If the matrix protein is anchored to a long chain of hyaluronan and is totally separated from the filtration sheet, no influence is expected for the effective oncotic pressure.

Participation of large and small pores in the water flux in the model

Morphological and physiological studies indicated multiple routes for substrate transport across capillary endothelium. However, the assignment of specific transport roles to morphologically identifiable pathways has been only partly achieved. The contributions of junctions, single vesicles, chains of vesicles and fenestrae to total macromolecular transport have been suggested, but their quantitative contributions are not yet known precisely [19]. Identification of the "small-pore" pathway for water and lipid-insoluble molecules still largely remains questionable. A theoretical approach from physics may be indispensable for understanding the mechanism of solute permeation through the glycocalyx sheet. Indeed, some of the theoretical calculations of parameters, optimized by fitting the experimental measurement of substrate flux, are explicitly related to the coefficients determined by Kedem and Katchalsky [7]. When the total flux through the capillary membrane is reconstructed, it might be necessary to adjust the ratio of different types of pores according to the experimental data. Rippe and Haraldsson suggested that 86–87% of the hydraulic conductivity (L_p) was accounted for by the small-pore pathway and 3.0–4.1% of L_p by the endothelial pathway, while the remaining fraction (10%) would be accounted for by a large-pore pathway [9]. On the other hand, Kellen and Bassingthwaighte (2003) [17], based on the osmotic weight transient data in isolated rabbit hearts, estimated that the endothelial pathway for transcapillary water-only exchange accounts for 28% of total transcapillary hydraulic conductivity, the large-pore pathway accounts for 5% of L_p, and the majority 67% is via a small-pore pathway [17]. In the present study, we simply referred directly to the experimental permeability coefficient determined for the whole area of capillary membrane (surface) without discriminating large and small pores.

Limitations of the present model

To get a deeper insight into the balance between glucose supply and glucose utilization by skeletal muscle, it might be important to replace the simple saturation kinetics [Eq. (1)] by a detailed metabolic pathway for glucose consumption in the skeletal muscle. We await the addition of mechanisms of physiologically active substances, such as serotonin and histamine [46] to the model, to further develop a physiological capillary model which can be applied to a variety of capillary functions in different tissues.

Acknowledgements We thank colleagues in the laboratory of Regulation of Tissue Functions at the Department of life Sciences, Ritsumeikan University, for very fruitful discussions.

Compliance with ethical standards

No experimental measurements were carried out in the present study.

Conflict of interest The authors declare that they have no conflict of interest.

References

1. Goldstein MS, Mullick V, Huddlestun B, Levine R (1953) Action of muscular work on transfer of sugars across cell barriers; comparison with action of insulin. Am J Physiol 173:212–216
2. Hansen P, Gulve E, Gao J, Schluter J, Mueckler M, Holloszy J (1995) Kinetics of 2-deoxyglucose transport in skeletal muscle: effects of insulin and contractions. Am J Physiol 268:C30–C35
3. Desvigne N, Barthelemy JC, Bertholon F, Gay-Montchamp JP, Freyssenet D, Costes F (2004) Validation of a new calibration method for human muscle microdialysis at rest and during exercise. Eur J Appl Physiol 92:312–320
4. Rosdahl H, Ungerstedt U, Jorfeldt L, Henriksson J (1993) Interstitial glucose and lactate balance in human skeletal muscle and adipose tissue studied by microdialysis. J Physiol 471:637–657
5. Henriksson J, Knol M (2005) A single bout of exercise is followed by a prolonged decrease in the interstitial glucose concentration in skeletal muscle. Acta Physiol Scand 185:313–320
6. Hamrin K, Henriksson J (2008) Interstitial glucose concentration in insulin-resistant human skeletal muscle: influence of one bout of exercise and of local perfusion with insulin or vanadate. Eur J Appl Physiol 103:595–603
7. Curry FE (1974) A hydrodynamic description of the osmotic reflection coefficient with application to the pore theory of transcapillary exchange. Microvasc Res 8:236–252
8. Renkin EM (1977) Multiple pathways of capillary permeability. Circ Res 41:735–743
9. Rippe B, Haraldsson B (1986) Capillary permeability in rat hindquarters as determined by estimations of capillary reflection coefficients. Acta Physiol Scand 127:289–303
10. Wolf MB (2002) A three-pathway pore model describes extensive transport data from mammalian microvascular beds and frog microvessels. Microcirculation 9:497–511
11. Michel CC (1980) Filtration coefficients and osmotic reflexion coefficients of the walls of single frog mesenteric capillaries. J Physiol 309:341–355
12. Pappenheimer JR, Renkin EM, Borrero LM (1951) Filtration, diffusion and molecular sieving through peripheral capillary membranes; a contribution to the pore theory of capillary permeability. Am J Physiol 167:13–46
13. Diana JN, Long SC, Yao H (1972) Effect of histamine on equivalent pore radius in capillaries of isolated dog hindlimb. Microvasc Res 4:413–437
14. Taylor AE, Gibson WH, Granger HJ, Guyton AC (1973) The interaction between intracapillary and tissue forces in the overall regulation of interstitial fluid volume. Lymphology 6:192–208
15. Miserocchi G, Negrini D, Mukenge S, Turconi P, Del Fabbro M (1989) Liquid drainage through the peritoneal diaphragmatic surface. J Appl Physiol (1985) 66:1579–1585
16. Kellen MR, Bassingthwaighte JB (2003) An integrative model of coupled water and solute exchange in the heart. Am J Physiol Heart Circ Physiol 285:H1303–H1316
17. Kellen MR, Bassingthwaighte JB (2003) Transient transcapillary exchange of water driven by osmotic forces in the heart. Am J Physiol Heart Circ Physiol 285:H1317–H1331
18. Bassingthwaighte JB, Raymond GM, Ploger JD, Schwartz LM, Bukowski TR (2006) GENTEX, a general multiscale model for in vivo tissue exchanges and intraorgan metabolism. Philos Trans A Math Phys Eng Sci 364:1423–1442
19. Li Y, Dash RK, Kim J, Saidel GM, Cabrera ME (2009) Role of NADH/NAD + transport activity and glycogen store on skeletal muscle energy metabolism during exercise: in silico studies. Am J Physiol Cell Physiol 296:C25–C46
20. Himeno Y, Ikebuchi M, Maeda A, Noma A, Amano A (2016) Mechanisms underlying the volume regulation of interstitial fluid by capillaries: a simulation study. Integr Med Res 5:11–21
21. Krogh A (1919) The number and distribution of capillaries in muscles with calculations of the oxygen pressure head necessary for supplying the tissue. J Physiol 52:409–415
22. Levick JR (2013) An introduction to cardiovascular physiology, chapter 10, 5th edn. CRC Press, Boca Raton, FL
23. Holloszy JO, Narahara HT (1965) Studies of tissue permeability. X. Changes in permeability to 3-methylglucose associated with contraction of isolated frog muscle. J Biol Chem 240:3493–3500
24. Park CR, Crofford OB, Kono T (1968) Mediated (nonactive) transport of glucose in mammalian cells and its regulation. J Gen Physiol 52:296–318
25. Furler SM, Jenkins AB, Storlien LH, Kraegen EW (1991) In vivo location of the rate-limiting step of hexose uptake in muscle and brain tissue of rats. Am J Physiol 261:E337–E347
26. Ziel FH, Venkatesan N, Davidson MB (1988) Glucose transport is rate limiting for skeletal muscle glucose metabolism in normal and STZ-induced diabetic rats. Diabetes 37:885–890
27. Glatz JF, Luiken JJ, Bonen A (2010) Membrane fatty acid transporters as regulators of lipid metabolism: implications for metabolic disease. Physiol Rev 90:367–417
28. Wallberg-Henriksson H, Holloszy JO (1984) Contractile activity increases glucose uptake by muscle in severely diabetic rats. J Appl Physiol Respir Environ Exerc Physiol 57:1045–1049
29. Karnieli E, Armoni M (2008) Transcriptional regulation of the insulin-responsive glucose transporter GLUT4 gene: from physiology to pathology. Am J Physiol Endocrinol Metab 295:E38–E45
30. Whitesell RR, Gliemann J (1979) Kinetic parameters of transport of 3-O-methylglucose and glucose in adipocytes. J Biol Chem 254:5276–5283
31. Guyton AC (1963) A concept of negative interstitial pressure based on pressures in implanted perforated capsules. Circ Res 12:399–414
32. Guyton AC (1965) Unterstitial fluid presure. II. Pressure-volume curves of interstitial space. Circ Res 16:452–460
33. Hamilton WF, Dow P (1963) Circulation. Handbook of physiology, Section 2. America Physiological Society, Washington, pp 961–1034
34. Hall JE (2015) Guyton and Hall textbook of medical physiology, chapter16. Elsevier Health Sciences, Philadelphia
35. Michel CC, Phillips ME (1987) Steady-state fluid filtration at different capillary pressures in perfused frog mesenteric capillaries. J Physiol 388:421–435
36. Landis EM (1934) Capillary pressure and capillary permeability. Physiol Rev 14:404–481
37. Renkin EM (1954) Filtration, diffusion, and molecular sieving through porous cellulose membranes. J Gen Physiol 38:225–243
38. Oberg CM, Rippe B (2014) A distributed two-pore model: theoretical implications and practical application to the glomerular sieving of Ficoll. Am J Physiol Renal Physiol 306:F844–F854

39. Renkin EM (ed) (1987) Handbook of physiology: Section 2. The cardiovascular system. Microcirculation: pt. 2, vol 4. American Physiological Society, Bethesda, MD, p 431
40. Korth U, Merkel G, Fernandez FF, Jandewerth O, Dogan G, Koch T, van Ackern K, Weichel O, Klein J (2000) Tourniquet-induced changes of energy metabolism in human skeletal muscle monitored by microdialysis. Anesthesiology 93:1407–1412
41. McDonald JN, Levick JR (1993) Effect of extravascular plasma protein on pressure-flow relations across synovium in anaesthetized rabbits. J Physiol 465:539–559
42. Michel CC (1997) Starling: the formulation of his hypothesis of microvascular fluid exchange and its significance after 100 years. Exp Physiol 82:1–30
43. Weinbaum S (1998) 1997 Whitaker Distinguished Lecture: models to solve mysteries in biomechanics at the cellular level; a new view of fiber matrix layers. Ann Biomed Eng 26:627–643
44. Adamson RH, Lenz JF, Zhang X, Adamson GN, Weinbaum S, Curry FE (2004) Oncotic pressures opposing filtration across non-fenestrated rat microvessels. J Physiol 557:889–907
45. Levick JR (1991) Capillary filtration-absorption balance reconsidered in light of dynamic extravascular factors. Exp Physiol 76:825–857
46. Michel CC, Kendall S (1997) Differing effects of histamine and serotonin on microvascular permeability in anaesthetized rats. J Physiol 501(Pt 3):657–662